Physical Communication 67 (2024) 102524

Contents lists available at ScienceDirect

Physical Communication

journal homepage: www.elsevier.com/locate/phycom

Full length article

Sum rate optimization in STAR-RIS assisted multiuser massive MIMO-OFDM VLC systems

M.A. Amirabadi [a,*], S.A. Nezamalhosseini [b]

[a] Department of Electrical Engineering, Ferdowsi University of Mashhad, Mashhad 9177948883, Iran
[b] School of Electrical Engineering, Iran University of Science and Technology (IUST), Tehran, 1684613114, Iran

ARTICLE INFO

Keywords:
Massive multiple input multiple output
Multiuser
Simultaneous transmission and reflection-reconfigurable intelligent surface
Sum rate
Visible light communication

ABSTRACT

Visible Light Communication (VLC) offers a promising solution for future networks, leveraging existing lighting infrastructure in indoor environments. However, VLC requires a direct line of sight to function which can be limiting. Reconfigurable Intelligent Surface (RIS) is a new technology that can bend light and radio waves, addressing this limitation in VLC. RIS come in three types: passive which reflects signals, active that boosts and reflects signals, and Simultaneous Transmission and Reflection (STAR)-RIS which can both reflect and transmit signals simultaneously. STAR-RIS offers the most control over the signal. In this paper, we propose a new multi-user VLC system with a massive Multiple-Input, Multiple-Output Orthogonal Frequency-Division Multiplexing (MIMO-OFDM) architecture, leveraging STAR-RIS to optimize data rates and improve coverage, particularly in non-line-of-sight scenarios. We formulate a system model and solve a convex optimization problem to determine the optimal transmission and reflection coefficients for STAR-RIS elements, aiming to maximize the total sum rate for all users. By employing maximum ratio transmission precoding, we minimize interference among users and demonstrate significant performance gains. Simulation results show that our proposed energy splitting-based STAR-RIS configuration outperforms traditional mode selection and time switching approaches with fixed or random coefficients, yielding substantial improvements in data rates and user experience. This study offers the first detailed exploration of STAR-RIS in VLC systems, highlighting its potential for future high-speed, multi-user communication networks. Our findings set the stage for further research into optimizing VLC systems using STAR-RIS, particularly in complex environments with non-line-of-sight users and massive MIMO-OFDM configurations.

1. Introduction

Visible Light Communication (VLC) is a subfield of optical wireless communication that utilizes the visible light spectrum for data transmission. A defining characteristic of VLC is its capability to seamlessly integrate data transmission with illumination. This enables imperceptible data transfer to the human eye, ensuring the surrounding environment remains lit as usual [1,2]. VLC leverages existing Light Emitting Diode (LED) lighting infrastructure. Due to the dual functionality of LEDs as illuminators and data transmitters, VLC eliminates the need for dedicated communication infrastructure. This translates to significant cost savings in deployment and maintenance. The visible light spectrum offers a substantial advantage over the Radio Frequency (RF) spectrum. Frequency allocation in the RF band is limited and tightly regulated due to diverse applications like military use, radio broadcasting, and Wi-Fi. In contrast, VLC utilizes the vast and unregulated visible light spectrum, opening doors for high-bandwidth applications in research and commercial sectors. VLC is susceptible to interference from various light sources. This includes other LEDs, traditional incandescent bulbs, and even sunlight. This sensitivity presents a significant challenge for reliable data transmission in VLC systems, requiring careful design considerations during deployment [1,2].

Multiuser massive Multiple Input Multiple Output (MIMO) VLC is a cutting-edge wireless communication technology that combines the capabilities of massive MIMO systems with the benefits of VLC to serve multiple users simultaneously. Utilizing large arrays of LEDs as transmitters and photodiodes as receivers enables high data throughput and increased network capacity by transmitting multiple data streams concurrently to different users. By exploiting the visible light spectrum, multiuser massive MIMO VLC offers high-speed, reliable, and secure communication, particularly advantageous for indoor environments. This technology holds significant promise for applications in high-density user scenarios, such as smart homes, offices, and public spaces, providing enhanced connectivity and performance [3].

* Corresponding author.
E-mail addresses: amirabadi@um.ac.ir (M.A. Amirabadi), nezam@iust.ac.ir (S.A. Nezamalhosseini).

https://doi.org/10.1016/j.phycom.2024.102524
Received 16 August 2024; Received in revised form 12 September 2024; Accepted 11 October 2024
Available online 18 October 2024

On the other hand, Orthogonal Frequency-Division Multiplexing (OFDM) is increasingly attractive for optical systems due to its superior power efficiency compared to traditional techniques like On-Off keying and pulse position modulation. However, a significant hurdle exists when directly applying conventional OFDM to Intensity Modulation/Direct Detection (IM/DD) optical wireless systems. Unlike traditional OFDM which transmits complex signals with potentially negative values, IM/DD systems are limited to real and non-negative signals. This inherent mismatch between OFDM signal characteristics and IM/DD system constraints necessitates alternative approaches to utilize OFDM benefits in this context. To overcome this limitation, three primary OFDM methods have been developed for IM/DD optical systems: Asymmetric clipped optical OFDM clips the negative portions of the OFDM signal, resulting in a real and positive signal suitable for IM/DD transmission. DC bias optical OFDM adds a constant positive bias (DC) to the entire OFDM signal, ensuring all values remain positive for IM/DD compatibility. Asymmetrically clipped DC biased optical OFDM utilizes a DC bias and asymmetric clipping to achieve a real, non-negative signal while potentially offering improved spectral efficiency compared to DC bias optical OFDM [4].

1.1. Literature review

To address line-of-sight blockages and enhance the communication channel environment for more reliable connections, Reconfigurable Intelligent Surfaces (RIS) have recently been introduced for use in both RF and VLC systems [5]. RIS technology is revolutionizing VLC systems by introducing a programmable environment [6]. These intelligent surfaces consist of low-cost, passive elements controlled by a central unit. This unit dynamically adjusts the phase and amplitude of each element, enabling precise manipulation of optical wave propagation. In VLC, RIS typically employs meta-surfaces or mirror arrays to direct the incident wave from the transmitter towards the desired destination, ensuring the reception of a strong signal. More specifically, conventional RIS can absorb, amplify, and reflect or transmit incoming waves in unconventional ways [5], thereby improving the spectral efficiency of the communication link. Due to these unique properties, RIS has become a subject of extensive research from various perspectives. For example, in [7], a liquid crystal-based structure is proposed for fabricating optical RIS. In [8], the authors calculate the irradiance of a photodetector in the presence of mirror array-based and meta-surface-based RIS. They also derive analytical expressions for the required phase gradient and reflector orientation in the cases of meta-surface-based and mirror array-based RIS, respectively. In [9], the channel model and delay spread for a RIS-assisted VLC system are developed. Furthermore, the authors in [10] establish lower and upper bounds for the capacity of VLC links with RIS, considering average optical power and peak-intensity constraints. In [11], a non-line-of-sight VLC link is examined, and the impact of RIS on this link is analyzed. Additionally, [12] investigates rate maximization for a single-user downlink VLC system with mirror array-based RIS under random user orientation and blockage conditions. In [13], a downlink MIMO VLC system is studied, where RIS is used to minimize the mean square error (MSE) of demodulated signals at the receiver. Another study in [14] looks at a cell-free RIS-assisted VLC network with L LEDs and K users, where the LEDs serve the users through time-division multiple access, and the system's sum-rate is maximized using a greedy algorithm. Energy efficiency optimization for a downlink RIS-assisted VLC system is explored in [15] by jointly optimizing time allocation, power control coefficients, and the phase shift matrix. In [16], the secrecy rate of a downlink RIS-aided VLC system in the presence of a legitimate user and an eavesdropper is derived and maximized, demonstrating how RIS can enhance the security of VLC links. Notably, [17] is the first to employ non-orthogonal multiple access techniques with RIS in VLC links, improving link quality under random user orientation and blockage while minimizing the maximum bit error rate for non-orthogonal multiple access users. Authors of [18] provided a comprehensive examination of how RIS can enhance the performance of VLC systems in vehicular environments. It offers a detailed channel model and performance metrics, demonstrating that IRS can significantly improve signal strength and reliability in such challenging scenarios.

A recent advancement in RIS technology, known as simultaneously transmitting and reflecting RIS (STAR-RIS), has been introduced for use in RF wireless systems [19,20]. As the name suggests, STAR-RIS can both reflect and transmit incoming waves, providing omnidirectional coverage [21]. This opens doors for even more sophisticated signal manipulation and network design possibilities [22,23]. Unlike multi-transmitter setups, STAR-RIS does not require a large number of LEDs to be deployed as data transmitters. It can leverage existing infrastructure by manipulating light from a smaller number of transmitters with reconfigurable surfaces. Compared to relays, STAR-RIS offers more refined control over the light signal. By reflecting and potentially transmitting simultaneously, STAR-RIS can focus the light towards receivers, reducing signal power wasted in unintended directions. This can improve data rates and reduce interference between users. A single STAR-RIS surface can manipulate light from multiple transmitters, offering more flexibility in network design. Additionally, the reconfigurable nature of STAR-RIS allows for adjustments to optimize signal delivery as user locations or network demands change [22,23]. STAR-RIS is rapidly gaining attention in RF-based wireless communication. The authors of [24] proposed a robust beamforming design for STAR-RIS-assisted secure transmission, addressing challenges related to imperfect channel state information and interference mitigation. Similarly, in [25], the focus was on robust beamforming for STAR-RIS-aided secure simultaneous wireless information and power transfer systems, also considering bounded channel state information errors. Both [24,25] tackle these issues by developing beamforming strategies to enhance the signal-to-interference-plus-noise ratio and reduce information leakage to eavesdroppers. In [26], the integration of RIS with mm-Wave integrated sensing and communication systems is explored. Meanwhile, the authors of [27] examined AI-enabled STAR-RIS for secure communications in multiple-input single-output interference alignment and cancellation systems. [28,29] investigate resource allocation problems in IRS-assisted wireless powered heterogeneous networks and IoT systems. Despite the progress in RF systems, the use of STAR-RIS in VLC systems remains underexplored across various use cases and perspectives. In [30], the fabrication method for an optical digital STAR-RIS is discussed, where the authors consider discrete phase shifts to implement a fully digital STAR-RIS for optical communications. Authors of [31] investigated performance improvements in non-orthogonal multiple access VLC systems using STAR-RIS. In the system model, a single STAR-RIS separates two rooms, an Access Point (AP) resides in the first room, and each room has one user. Achievable user rates are obtained for two data retrieval techniques: single user detection and sequential interference cancellation. The sum rate optimization problem is formulated for two STAR-RIS operating modes: energy sharing and mode switching. In [32], authors investigated an OFDM-based MIMO system for VLC using an LED array for data transmission. Three precoding methods, including Maximum Ratio Transmission (MRT), Zero-forcing (ZF), and Minimum Mean Square Error (MMSE) within the context of IM/DD have been studied in [32]. In [33,34], the use of optical RIS is considered to enhance MIMO VLC performance, focusing on minimizing the receiver's mean squared error and the impact of RIS-induced time delays on the VLC channel's frequency domain characteristics. Authors of [35–37] analyzed various aspects of VLC systems without STAR-RIS, including precoding techniques and user scheduling.

1.2. Novelties and contributions

This paper introduces a novel approach for high-speed, multi-user VLC systems. It leverages intelligent reflecting surfaces, STAR-RIS, to

enhance performance, enabling massive MIMO-OFDM for significant data rate improvements. We establish a system model and employ precoding techniques to minimize interference between multiple users. The core challenge addressed is maximizing the total data rate for all users in massive MIMO VLC systems, an area with limited exploration in previous research. To achieve this, we formulate and solve a mathematical optimization problem to determine the optimal settings for reflecting and transmitting signals off the STAR-RIS elements. Simulations validate that this optimized configuration significantly outperforms less effective approaches. Unlike prior works, we consider scenarios where users are not directly in line-of-sight with the access point, reflecting a more realistic deployment. This research opens doors for further investigation into optimizing communication performance in non-orthogonal multiple access VLC systems with STAR-RIS. Our findings are particularly relevant for scenarios involving non-line-of-sight users and massive MIMO configurations, paving the way for improved user experience in future VLC systems. Therefore, this paper introduces several novel contributions to the field of VLC systems, specifically through the application of STAR-RIS. Here are the key novelties and contributions:

- The paper explores the use of STAR-RIS in VLC systems, an area that has not been widely investigated before. This approach allows the surface to both reflect and transmit light, which can enhance coverage and improve signal quality.
- The research presents a system model for high-speed, multi-user VLC systems that leverages STAR-RIS to enable massive MIMO-OFDM configurations. This setup is aimed at significantly improving data rates by reducing interference among multiple users. This combination of massive MIMO and OFDM with STAR-RIS is a unique contribution to the field.
- The paper establishes a system model for massive MIMO-OFDM VLC with STAR-RIS and employs precoding techniques to minimize interference between users.
- The paper focuses on maximizing the total data rate for all users in the system, a challenging problem that has not been extensively explored in previous research. It does so by formulating and solving a mathematical optimization problem to determine the optimal settings for STAR-RIS elements, which improves signal transmission and reflection.
- Unlike previous research, this study considers scenarios where users are not directly in line-of-sight with the access point. This adds a layer of realism to the deployment and showcases the potential of STAR-RIS to enhance VLC system performance even in more challenging environments.
- The paper validates its proposed approach through simulations, demonstrating that the optimized STAR-RIS configuration significantly outperforms less effective methods. This provides strong evidence of the practical benefits of using STAR-RIS in VLC systems.
- The research opens the door for further investigation into optimizing communication performance in non-orthogonal multiple access VLC systems with STAR-RIS, particularly in scenarios involving non-line-of-sight users and massive MIMO configurations.

There are two main approaches to controlling STAR-RIS elements: phase-shifting and Binary (0-1). Phase-shifting approach allows for more precise control by assigning specific phase shifts to each element, enabling more sophisticated beamforming techniques. Binary (0-1) represents a simpler approach where each element acts as a perfect reflector (1) or perfect absorber (0). While offering ease of implementation, it limits the flexibility in manipulating the signal phase. Beyond these control methods, there are three main practical protocols for STAR-RIS operation: energy splitting, mode selection, and time switching. Energy splitting divides the incident signal into two parts: one for reflection and the other for transmission. This allows for flexible control of the reflected and transmitted signals. In mode selection protocol, the STAR-RIS can switch between different operating modes (e.g., only reflecting, only transmitting, or a combination) based on the specific requirements of the communication scenario. Time switching method involves switching between reflection and transmission modes in time slots. It can be used to allocate resources efficiently and manage interference [38–40]. In our model, we have adopted the energy splitting protocol for the STAR-RIS while optimization. We applied mode selection and time switching scenarios as benchmarks to highlight the contribution of this work using energy splitting for STAR-RIS. Each protocol offers trade-offs in terms of energy efficiency, spectral efficiency, and system complexity. By comparing energy splitting against mode selection and time switching, we can show how energy splitting maximizes resource utilization and system performance. Mode selection and time switching are practical and simpler approaches, making them realistic baselines for evaluating the effectiveness of your more complex energy splitting approach.

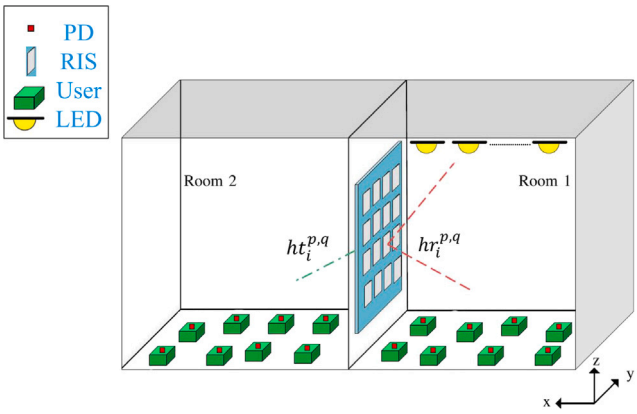

Fig. 1. Considered STAR-RIS assisted multiuser massive MIMO VLC System.

The rest of the paper is organized as follows; Section 2 establishes the foundational elements of the research by detailing the system model, including user distribution, and relevant parameters. The channel model for the multiuser massive MIMO-OFDM VLC system with STAR-RIS assistance is presented in Section 3. This model incorporates relevant factors like path loss, reflection coefficients, and time delays. Section 4 delves into the operational principles of the multiuser massive MIMO VLC system. It elaborates on signal transmission, and receiver processing strategies. The optimization problem for maximizing the system's overall data rate (sum rate) is formulated and subsequently solved in Section 5. The employed optimization techniques and any relevant constraints are also discussed. Section 6 presents the simulation results obtained by applying the proposed system model, channel model, and optimization solution. The results evaluate the impact of various system parameters on data rate. Section 7 summarizes the key findings of the research, highlighting the contributions to the field of massive MIMO VLC with STAR-RIS.

2. System model

The considered system model is depicted in Fig. 1. The scenario considers two rooms separated by a STAR-RIS. In the first room, an AP with M LEDs transmits to L users. The second room has $N - L$ users but no transmitters. All communication relies on indirect paths reflected or transmitted by the STAR-RIS. Each STAR-RIS element can reflect signals from LEDs, coefficient $\alpha, 0 \leq \alpha \leq 1$, towards users in the first room, simultaneously transmit the same signals, coefficient $\beta = 1-\alpha$, towards users in the second room. We assume no line-of-sight exists between LEDs and users, M LEDs and N photodetectors (PDs) utilize spatial multiplexing with identical specifications, and user PD heights are fixed on a screen at a specific distance from the floor. Time

delays are introduced due to varying distances between users, STAR-RIS elements, and LEDs. These delays are considered in the channel model to manipulate channel correlation in the frequency domain. Thermal noise, shot noise, background noise, and dark current noise can corrupt the received signal at the PDs, impacting system performance. The combined effect of these noise sources can be approximated by a Gaussian distribution with zero mean. The variance of the Gaussian noise of the pth user is calculated as follows [32,35]:

$$\sigma_p^2 = 2eP_p^{opt}B + 2e\gamma_p X_{amb} A_p^{PD}(1 - cos(k_p)) + i_{amp}^2 B \tag{1}$$

where e is the electronic charge, X_{amb} is the ambient light photocurrent, B is signal bandwidth, and i_{amp} is the preamplifier noise current density. The parameters A_p^{PD} is PD area, γ_p is PD responsivity coefficient, k_p is receiver half-angle, P_p^{opt} is the average received optical power at the pth user.

Assuming identical parameter values across users, we set $\sigma^2 = \sigma_p^2$ in the following.

3. Channel model

3.1. Channel model in the first room

Signal paths from LEDs and STAR-RIS elements to each user introduce time delays. These variations depend on the specific location of the user relative to the transmitters and the STAR-RIS. Consequently, the sum of channels in the time domain between the pth user and the qth transmitter in the first room can be expressed as [31,32]

$$h^{p,q}(t) = \sum_{i=1}^{I} \alpha_i hr_i^{p,q} \delta(t - t_i^{p,q}) \tag{2}$$

where α_i represents the reflection coefficient of the ith element of the STAR-RIS. This value determines the strength of the signal reflected by that element. I represents the total number of elements within the STAR-RIS. $t_i^{p,q}$ represents the time delay experienced by the signal from the qth LED after reflection by the ith element of the STAR-RIS before reaching the pth user. This delay accounts for the indirect path the signal takes due to reflection. $hr_i^{p,q}$ represents the channel response for the indirect line-of-sight path between the qth LED and the pth user via the ith element of the STAR-RIS in the first room and can be expressed as [31,32]

$$hr_i^{p,q} = \frac{A_p^{PD}(m+1)}{2\pi(d_{q,i} + d_{i,p})^2} cos(\varphi_{q,i})^m cos(\Psi_{i,p}) G_p \times 1_{k_p}(0 \le \Psi_{i,p} \le \Psi_c) \tag{3}$$

where $\varphi_{q,i}$, aadiation angles, represent the direction of light propagation from the qth LED to the ith element of the STAR-RIS. $\Psi_{i,p}$, collision angles, represent the direction of light propagation from the ith element of the STAR-RIS towards the pth user. A_p^{PD}, PD surface area, accounts for the effective area of the PD at the pth user that captures the received light signal. Ψ_c, receiver field of view, defines the angular range within which the optical receiver at the pth user can detect light signals. The Lambertian emission order, m, characterizes the angular emission pattern of the light source (LEDs in this case) and can be written as [31,32]

$$m = -\frac{ln(2)}{ln(cos(\Psi_{\frac{1}{2}}))} \tag{4}$$

where $\Psi_{\frac{1}{2}}$ represents the half-power angle of the LED which is the angle at which the light intensity drops to half of its peak value.

The frequency domain impulse response of the channel between the pth user and the qth transmitter for the kth subcarrier in the first room, denoted as $H_k^{p,q}$, can be expressed as

$$H_k^{p,q} = \sum_{i=1}^{I} \alpha_i hr_i^{p,q} exp\left(\frac{-j2\pi k B t_i^{p,q}}{K}\right) \tag{5}$$

where K represents the total number of subcarriers used in the optical OFDM system.

3.2. Channel model in the second room

The channel model for the second room shares similarities with the first room. However, a crucial difference lies in the reflection coefficients used. First Room: Reflection coefficients for the STAR-RIS elements are employed. Second Room: Transmission coefficients for the STAR-RIS elements are employed, as the signal is directly transmitted from the RIS to the users in the second room. Consequently, the sum of the channels in the time domain between the pth user and the qth transmitter in the second room can be expressed as [31,32]

$$h^{p,q}(t) = \sum_{i=1}^{I} \beta_i ht_i^{p,q} \delta(t - t_i^{p,q}). \tag{6}$$

Similar to the first room, $H_k^{p,q}$ represents the frequency domain impulse response of the channel between the pth user and the qth transmitter for the kth subcarrier in the second room. This response can be expressed as

$$H_k^{p,q} = \sum_{i=1}^{I} \beta_i ht_i^{p,q} exp(\frac{-j2\pi k B t_i^{p,q}}{K}) \tag{7}$$

where

$$ht_i^{p,q} = \frac{A_p^{PD}(m+1)}{2\pi(d_{q,i} + d_{i,p})^2} cos(\varphi_{q,i})^m cos(\Psi_{i,p}) G_p \times 1_{k_p}(0 \le \Psi_{i,p} \le \Psi_c). \tag{8}$$

While the time delay between users and LEDs within a confined room is typically small, analyzing time delay remains an important consideration for several reasons; In complex environments such as STAR-RIS with multiple transmissions and reflections, time delay can lead to multipath effects, which can further degrade system performance. By analyzing time delay, we can gain insights into the impact of these effects and develop strategies to mitigate them. While our current focus is on indoor VLC systems, future applications might involve larger-scale deployments or scenarios with longer distances between transmitters and receivers. In these cases, time delay could become a more significant factor affecting system performance. As VLC systems are increasingly used for high-speed data transmission, even small time delays can introduce inter-symbol interference and degrade the overall data rate. Analyzing time delay helps us understand the limitations of VLC systems and identify potential mitigation techniques.

4. Multiuser massive MIMO OFDM-based data transmission

The block diagram in Fig. 2 illustrates a multiuser massive MIMO-OFDM system. An array of M LEDs acts as transmitters. N users are equipped with PDs for signal reception. The system utilizes optical OFDM to achieve high spectral efficiency. The system commences by mapping each user's binary data stream into a sequence of symbols, denoted by S_k^p. The specific symbol chosen for a particular pth user on a kth subcarrier depends on the chosen modulation scheme, e.g., quadrature amplitude modulation. To minimize interference between user signals, a precoding technique is applied on the AP side. This involves multiplying each user's symbol S_k^p by a user-specific precoding vector $W_k^{p,q}$. The precoding vector is specific to both the pth user and the qth LED transmitting the symbol on kth subcarrier. Since a STAR-RIS element with size I scatters each transmitted symbol through I distinct channels, the precoding vector $W_k^{p,q}$ has a length of I This ensures proper precoding for all the channels created by the STAR-RIS element. Following precoding for all N users' symbols in kth subcarrier and qth LED (both in the frequency domain), the resulting composite transmitted signal can be mathematically expressed as

$$X_k^q = \sum_{p=1}^{N} \sum_{i=1}^{I} W_k^{p,i,q} S_k^p, k = 0, 1, \dots, K-1, q = 1, \dots, M. \tag{9}$$

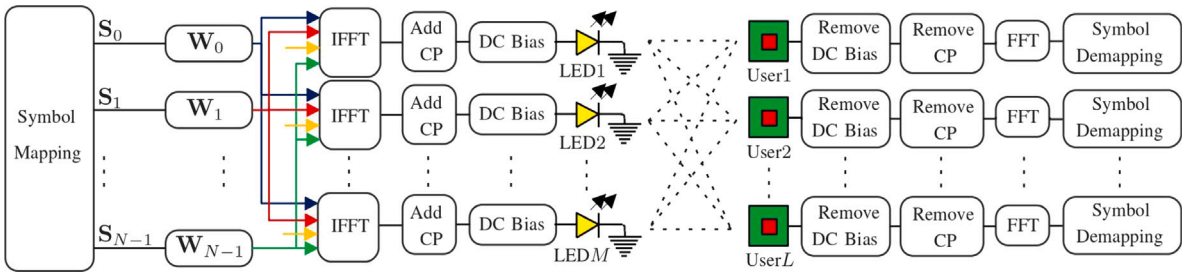

Fig. 2. The signal processing block diagram of STAR-RIS assisted multiuser massive MIMO VLC system.

After applying the Inverse Fast Fourier Transform to the precoded signal in the frequency domain, the transmitted signal for the qth LED in the time domain is obtained as

$$x_n^q = \frac{1}{\sqrt{K}} \sum_{k=0}^{K-1} X_k^q exp(\frac{j2\pi kn}{K}), n = 0, 1, \ldots, K-1. \tag{10}$$

To prevent inter-symbol interference at the receiver, a cyclic prefix is added to the beginning of each OFDM symbol in the time domain. The cyclic prefix replicates a portion of the symbol's end, creating a guard interval between symbols. This ensures that overlapping tails of previous symbols do not interfere with the beginning of subsequent symbols. Our system employs IM/DD for signal transmission. This technique requires the LEDs to emit a positive-valued signal. Therefore, a DC bias is added to the transmitted signal in the time domain before transmission. At each user's PD, the received optical signal is converted into its corresponding electrical signal. The following steps occur at the receiver: The DC bias added for transmission is removed, the cyclic prefix appended at the transmitter is discarded to remove the guard interval, the remaining signal is processed using the fast Fourier transform to convert it from the time domain back to the frequency domain. Following these processing steps, the symbols received by the pth user in the kth subcarrier in the frequency domain can be expressed as

$$Y_k^p = \gamma \sum_{q=1}^{M} \sum_{i=1}^{I} H_k^{p,i,q} X_k^q + Z_k^p \tag{11}$$

where

$$\begin{aligned} Y_k^p = \gamma &\sum_{q=1}^{M} \sum_{i=1}^{I} H_k^{p,i,q} W_k^{p,i,q} S_k^p \\ &+ \gamma \sum_{q=1}^{M} \sum_{\substack{l=1 \\ l \neq p}}^{N} \sum_{i=1}^{I} H_k^{p,i,q} W_k^{p,i,l} S_k^{l,p} + Z_k^p. \end{aligned} \tag{12}$$

The equation for the received symbols can be broken down into two key parts: The first part represents the intended signal for each user. This component incorporates: Precoded user symbol S_k^p transmitted on kth subcarrier for pth user, precoding vector $W_k^{p,q}$ applied to the user's symbol for qth LED, channel response $H_k^{p,i,q}$ between pth user, the ith STAR-RIS element, and qth LED for kth subcarrier. This term accounts for the effects of signal propagation on the desired path. The second part represents the combined interference from other users' signals. This interference arises due to imperfect channel isolation and can degrade the desired signal. The term Z_k^p represents noise affecting the received signal in kth subcarrier for pth user. This noise is typically modeled as a zero-mean Gaussian distribution with variance σ^2. To ensure the total transmitted power from all M LEDs on the AP remains constant, a scaling factor γ is applied to the signal sent by each LED. This factor essentially adjusts the power level of individual LED transmissions while maintaining the overall power budget.

Multiuser massive MIMO VLC systems often leverage linear precoding techniques to improve performance. Three prominent techniques are: MRT aims to maximize the received signal strength for each user while minimizing the impact of channel noise, ZF focuses on completely eliminating inter-user interference between user signals, and MMSE attempts to strike a balance between maximizing signal strength and minimizing both noise and inter-user interference. We employ the MRT precoding technique to address inter-user interference. MRT prioritizes enhancing the desired signal strength for each user while acknowledging the presence of noise. The MRT precoding matrix, as referenced in [32], is used to implement this technique. The specific form of this matrix will be presented as

$$W_k = \xi_k A_k \tag{13}$$

where

$$A_k = H_k^H. \tag{14}$$

The MRT precoding matrix relies on the channel information between the transmitter and receivers for kth subcarrier. This information is captured in the Hermitian matrix $A_k^H A_k$ where A_k represents the channel matrix for kth subcarrier. To ensure the precoding process does not alter the overall transmitted power, a scaling factor ξ_k is introduced. This factor is calculated as $\xi_k = \frac{1}{sqrt(tr(A_k^H A_k))}$ [32]. Here, $tr(A_k^H A_k)$ represents the trace of the Hermitian matrix which is the sum of its diagonal elements. By incorporating the MRT precoding matrix and the scaling factor, the formula for the received signal by the pth user in the kth subcarrier (originally formula (12)) can be rewritten as

$$\begin{aligned} Y_k^p = \gamma \xi_k &\sum_{q=1}^{M} \sum_{i=1}^{I} H_k^{p,i,q} A_k^{p,i,q} S_k^p \\ &+ \gamma \xi_k \sum_{q=1}^{M} \sum_{\substack{l=1 \\ l \neq p}}^{N} \sum_{i=1}^{I} H_k^{p,i,q} A_k^{p,i,l} S_k^{l,p} + Z_k^p. \end{aligned} \tag{15}$$

This revised formula now explicitly includes the MRT precoding matrix W_k and the scaling factor ξ_k, demonstrating how these elements influence the received signal. Building upon the relationship established in Eq. (14), we can express the channel and precoding components of the desired signal differently for the first and second rooms: The desired signal component in the first room can be rewritten by separating the channel response and the precoding applied by the MRT matrix. Similarly, the desired signal component in the second room can be expressed by separating the channel response which differs due to transmission through the RIS and the precoding applied by the MRT matrix. The specific mathematical rewrites for the desired signal components in both rooms will be presented as follows:

$$\sum_{q=1}^{M} \sum_{i=1}^{I} H_k^{p,i,q} A_k^{p,i,q} = \sum_{q=1}^{M} \sum_{i=1}^{I} (\alpha_i h r_i^{p,q})^2 \tag{16}$$

$$\sum_{q=1}^{M} \sum_{i=1}^{I} H_k^{p,i,q} A_k^{p,i,q} = \sum_{q=1}^{M} \sum_{i=1}^{I} (\beta_i h t_i^{p,q})^2. \tag{17}$$

Several studies, including [32], have shown that as the number of LEDs in a massive MIMO system approaches infinity, the MRT precoding technique becomes highly effective in eliminating interference between users. In this work, we consider a system with a large number of LEDs. Therefore, we can safely assume that the impact of user interference on

the overall system performance is negligible. Consequently, we simplify the optimization problem by neglecting the user interference term.

5. Sum rate optimization

The total data rate achievable by the system, also known as the sum rate, for N users in the kth subcarrier can be expressed as follows [41]

$$R_k = \sum_{p=1}^{N} \frac{1}{2} log_2(1 + \frac{e}{2\pi} SNR_k^p) \tag{18}$$

where

$$SNR_k^p = \frac{\gamma^2 \xi_k^2 |\sum_{q=1}^{M} \sum_{i=1}^{I} H_k^{p,i,q} A_k^{p,i,q}|^2}{\sigma^2}. \tag{19}$$

Building on the relationships established in Eqs. (16) and (17), we can express Eq. (19) in two equivalent forms: A specific form applies for the first room where the relevant factors like channel response and precoding differ from the second room. Another form applies for the second room, reflecting the distinct channel characteristics due to transmission through the RIS element. The specific rewrites for Eq. (19) in both rooms will be presented as follows

$$SNR_k^p = \frac{\gamma^2 \xi_k^2 (\sum_{q=1}^{M} \sum_{i=1}^{I} (\alpha_i hr_i^{p,q})^2)^2}{\sigma^2} \tag{20}$$

$$SNR_k^p = \frac{\gamma^2 \xi_k^2 (\sum_{q=1}^{M} \sum_{i=1}^{I} (\beta_i ht_i^{p,q})^2)^2}{\sigma^2} \tag{21}$$

Eqs. (20) and (21) demonstrate that the terms relevant to optimizing the system, maximizing the sum rate by adjusting the STAR-RIS coefficients, are independent of the specific subcarrier being used k. This means that factors like the Signal-to-Noise Ratio (SNR) experienced by each pth user do not vary depending on the subcarrier. As a result of this subcarrier independence, the optimization problem can be simplified. Instead of considering the SNR for each subcarrier SNR_k^p, we can use a single term representing the overall SNR experienced by each user SNR^p. This reduces the complexity of the optimization process. We formulate the optimization problem as

$$\underset{\alpha,\beta}{\text{Maximize}} \quad \sum_{p=1}^{N} \frac{1}{2} log_2(1 + \frac{e}{2\pi} SNR^p) \tag{22a}$$

$$\text{subject to} \quad 0 \le \alpha_i \le 1, i = 1, \dots, I \tag{22b}$$

$$0 \le \beta_i \le 1, i = 1, \dots, I \tag{22c}$$

$$\alpha_i + \beta_i = 1, i = 1, \dots, I \tag{22d}$$

Eqs. (20) and (21) involve variables raised to the power of two, making the optimization problem formulated in Eq. (22) non-convex. In simpler terms, the problem does not have a single, well-defined optimum point for the objective function. To address this challenge and make the problem more tractable, we introduce a new variable. This variable, denoted by t_p, represents a lower bound, maximum acceptable value, for the SNR experienced by each user (p).

$$\underset{\alpha,\beta,t}{\text{Maximize}} \quad \sum_{p=1}^{N} \frac{1}{2} log_2(1 + \frac{e}{2\pi} t_p) \tag{23a}$$

$$\text{subject to} \quad t_p \le \frac{\gamma^2 (\sum_{q=1}^{M} \sum_{i=1}^{I} (\alpha_i hr_i^{p,q})^2)^2}{(\sigma)^2}, p = 1, \dots, L \tag{23b}$$

$$t_p \le \frac{\gamma^2 (\sum_{q=1}^{M} \sum_{i=1}^{I} (\beta_i ht_i^{p,q})^2)^2}{(\sigma)^2}, p = L+1, \dots, N \tag{23c}$$

$$0 \le \alpha_i \le 1, i = 1, \dots, I \tag{23d}$$

$$0 \le \beta_i \le 1, i = 1, \dots, I \tag{23e}$$

$$\alpha_i + \beta_i = 1, i = 1, \dots, I \tag{23f}$$

In the next step, we focus on the lower limits (minimum acceptable values) represented by $\lambda_{p,i,q}$. These limits are associated with the squared terms of two key factors: $(\alpha_i hr_i^{p,q})^2$ term incorporates the reflection coefficient of the ith STAR-RIS element and the channel response ($hr_i^{p,q}$) between the pth user, the ith element, and the transmitting qth LED. $(\beta_i ht_i^{p,q})^2$ term involves the transmission coefficient of the ith element and the channel response $ht_i^{p,q}$ for direct transmission from the RIS element to the pth user.

$$\underset{\alpha,\beta,t,\lambda}{\text{Maximize}} \quad \sum_{p=1}^{N} \frac{1}{2} log_2(1 + \frac{e}{2\pi} t_p) \tag{24a}$$

$$\text{subject to} \quad t_p \le \frac{\gamma^2 (\sum_{q=1}^{M} \sum_{i=1}^{I} \lambda_{p,i,q})^2}{(\sigma)^2}, p = 1, \dots, N \tag{24b}$$

$$\lambda_{p,i,q} \le (\alpha_i hr_i^{p,q})^2, \quad p = 1, \dots, L, \ q = 1, \dots, M, \ i = 1, \dots, I \tag{24c}$$

$$\lambda_{p,i,q} \le (\beta_i ht_i^{p,q})^2, \quad p = L+1, \dots, N, \ q = 1, \dots, M, \ i = 1, \dots, I \tag{24d}$$

$$0 \le \alpha_i \le 1, i = 1, \dots, I \tag{24e}$$

$$0 \le \beta_i \le 1, i = 1, \dots, I \tag{24f}$$

$$\alpha_i + \beta_i = 1, i = 1, \dots, I \tag{24g}$$

To incorporate the newly defined lower limits for power levels, we will reformulate the original equations (24). The revised versions of these equations will be presented as follows

$$\underset{\alpha,\beta,t,\lambda}{\text{Maximize}} \quad \sum_{p=1}^{N} \frac{1}{2} log_2(1 + \frac{e}{2\pi} t_p) \tag{25a}$$

$$\text{subject to} \quad t_p - \frac{\gamma^2 (\sum_{q=1}^{M} \sum_{i=1}^{I} \lambda_{p,i,q})^2}{(\sigma)^2} \le 0, p = 1, \dots, N \tag{25b}$$

$$\lambda_{p,i,q} - (\alpha_i hr_i^{p,q})^2 \le 0, \quad p = 1, \dots, L, \ q = 1, \dots, M, \ i = 1, \dots, I \tag{25c}$$

$$\lambda_{p,i,q} - (\beta_i ht_i^{p,q})^2 \le 0, \quad p = L+1, \dots, N, \ q = 1, \dots, M, \ i = 1, \dots, I \tag{25d}$$

$$0 \le \alpha_i \le 1, i = 1, \dots, I \tag{25e}$$

$$0 \le \beta_i \le 1, i = 1, \dots, I \tag{25f}$$

$$\alpha_i + \beta_i = 1, i = 1, \dots, I \tag{25g}$$

Eqs. (25b), (25c), and (25d) still contain some elements that make solving the optimization problem difficult. To address this, we will leverage a mathematical technique called the first-order Taylor expansion. This technique essentially approximates a function around a specific point using a linear function. By applying this approach, we can transform these equations into a more tractable form, making the optimization problem convex.

$$\underset{\alpha,\beta,t,\lambda}{\text{Maximize}} \quad \sum_{p=1}^{N} \frac{1}{2} log_2(1 + \frac{e}{2\pi} t_p) \tag{26a}$$

$$\text{subject to} \quad t_p - \frac{\gamma^2}{\sigma^2}((\sum_{q=1}^{M} \sum_{i=1}^{I} \lambda_{p,i,q}^{(j)})^2 + 2(\sum_{q=1}^{M} \sum_{i=1}^{I} \lambda_{p,i,q}^{(j)}) ((\sum_{q=1}^{M} \sum_{i=1}^{I} \lambda_{p,i,q}) - (\sum_{q=1}^{M} \sum_{i=1}^{I} \lambda_{p,i,q}^{(j)}))) \le 0, p = 1, \dots, N \tag{26b}$$

$$\lambda_{p,i,q} - (\alpha_i^{(j)} hr_i^{p,q})^2 - 2(\alpha_i^{(j)} hr_i^{p,q})(\alpha_i hr_i^{p,q} - \alpha_i^{(j)} hr_i^{p,q}) \le 0, \quad p = 1, \dots, L, \ q = 1, \dots, M, \ i = 1, \dots, I \tag{26c}$$

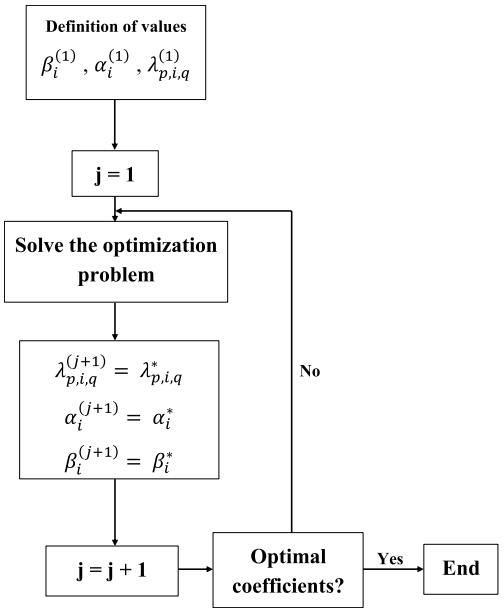

Fig. 3. The repetition algorithm to find the optimal STAR-RIS coefficient values for maximizing system performance.

$$\lambda_{p,i,q} - (\beta_i^{(j)} ht_i^{p,q})^2 - 2(\beta_i^{(j)} ht_i^{p,q})(\beta_i ht_i^{p,q} - \beta_i^{(j)} ht_i^{p,q}) \le 0 \,, \quad p = L+1, \dots, N,\ q = 1, \dots, M,\ i = 1, \dots, I \tag{26d}$$

$$0 \le \alpha_i \le 1, i = 1, \dots, I \tag{26e}$$

$$0 \le \beta_i \le 1, i = 1, \dots, I \tag{26f}$$

$$\alpha_i + \beta_i = 1, i = 1, \dots, I \tag{26g}$$

By applying the Taylor series expansion, we have transformed the optimization problem into a convex form [42–44]. This means the problem has a well-defined optimal solution that maximizes the sum rate. To find this optimal solution, the optimization problem formulated in Eqs. (26) can be tackled using an iterative algorithm. This algorithm will systematically adjust the STAR-RIS coefficients to progressively improve the sum rate while adhering to the defined constraints.

Fig. 3 details the iterative process of the repetition algorithm used to find the optimal values for the STAR-RIS coefficients. This algorithm progressively adjusts these coefficients to maximize the system's overall data rate.

Step 1, Initialization: Define initial values for three key parameters; $\lambda_{p,i,q}^{j}$, the lower limits for signal power levels at each jth iteration; $\alpha_i^{(j)}$, reflection coefficients of the ith STAR-RIS element at jth iteration; $\beta_i^{(j)}$, transmission coefficients of the ith STAR-RIS element at jth iteration. Here, it is crucial to ensure the sum of $\alpha_i^{(j)}$ and $\beta_i^{(j)}$ always equals one, as they represent the total power distribution.

Step 2, Optimization: Solve the optimization problem formulated in Eqs. (26) using the current values of $\lambda_{p,i,q}^{(j)}$, $\alpha_i^{(j)}$, and $\beta_i^{(j)}$.

Step 3, Update: Replace the current values of $\lambda_{p,i,q}$, α_i, and β_i with the solutions obtained from step 2. These become $\lambda_{p,i,q}^{(j+1)}$, $\alpha_i^{(j+1)}$, and $\beta_i^{(j+1)}$ for the next iteration.

Step 4, Convergence: Repeat steps 2 and 3 until the difference in the calculated sum rate between two consecutive iterations j+n and j+n-1 falls below the predefined threshold ϵ. This indicates that the algorithm has converged to a near-optimal solution.

Outcome: By iteratively refining the STAR-RIS coefficients through this process, the repetition algorithm achieves a configuration that maximizes the system's sum rate while ensuring minimum signal quality levels for the users.

Table 1
Simulation parameters.

Parameter	Symbol	Value
Room dimensions	[L, W, H]	$5 \times 5 \times 3$ m^3
Location of STAR-RIS center	[L, W, H]	[5 m, 2.5 m, 1.5 m]
STAR-RIS dimensions	[L, W, H]	[0 , 3 m, 2 m]
LED's half-angle	$\phi_{1/2}$	70°
Light speed	C	$3 \times 1e8$
Electronic charge	e	1.602e−19
PD area	A_p^{PD}	1 cm^2
PD responsivity coefficient	γ_p	0.4 A/W
Receiver half-angle	k_p	60°
Preamplifier noise current density	i_{amp}	5 pA/Hz$^{-1/2}$
Ambient light flow	X_{amp}	10.93 A/m^2/Sr
Signal bandwidth	B	1 GHz
Number of OFDM subcarriers	K	64
Number of LEDs	M	64
Number of Users	N	16
Number of STAR-RIS	I	35

5.1. Complexity analysis

To estimate the computational complexity of solving the optimization problem (26) using the CVX package [45], we need to examine the structure of the objective function, the constraints, and the number of variables.

The objective function (26a) is concave (logarithms are concave), and computing it involves evaluating the log term for each t_p, where $p = 1, \dots, N$. Thus, the complexity of the objective function is linear in N, i.e. $O(N)$.

First constraint (26b) is quadratic in the terms involving $\lambda_{p,i,q}$. The complexity arises from evaluating double sums over M (number of LEDs) and I (number of STAR-RIS elements), which gives complexity $O(M \times I)$ for each user p. Given that this constraint is applied for each user $p = 1, \dots, N$, the total complexity for this constraint becomes $O(N \times M \times I)$.

Second and third constraints (26c) and (26d) are quadratic constraints involving both $\lambda_{p,i,q}$, α_i, and β_i. Evaluating these requires quadratic terms for each pair (p, i, q), with a complexity of $O(1)$ for each pair. The complexity for each constraint is $O(M \times I)$ for each user p, and since there are L users for the second constraint and $N - L$ users for the third, the total complexity for both is $O(N \times M \times I)$.

The remaining constraints (26e), (26f), and (26g) are simple linear inequalities and equalities. These are $O(I)$ since they only affect the variables α_i and β_i.

The decision variables are: α_i and β_i, indexed by $i = 1, \dots, I$, so there are $O(I)$ variables. t_p, indexed by $p = 1, \dots, N$, so there are $O(N)$ variables. $\lambda_{p,i,q}$, indexed by $p = 1, \dots, N$, $i = 1, \dots, I$, and $q = 1, \dots, M$, so there are $O(N \times I \times M)$ variables.

CVX solvers (such as interior-point methods) have worst-case complexity $O(n^3)$, where n is the number of variables and constraints. For this problem, the number of variables is $O(N \times I \times M)$, so the solver complexity is $O((N \times I \times M)^3)$.

Therefore, the overall computational complexity is dominated by the solver's cubic complexity $O((N \times I \times M)^3)$. This is the worst-case complexity for solving the problem using CVX, where N, M, and I are the dominant factors.

6. Simulation results

In this section, we present the simulation results obtained by applying the proposed system model, channel model, and optimization solution. The results evaluate the impact of various system parameters on sum rate. Having established the optimization system and its solution approach in the previous section, we now turn our attention to analyzing its performance. To evaluate the effectiveness of the proposed

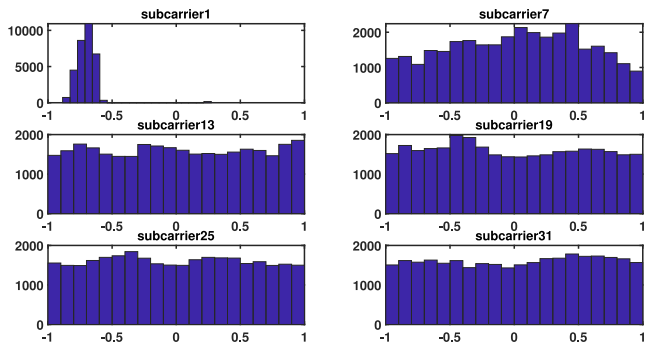

Fig. 4. Channel phase histogram for different subcarriers.

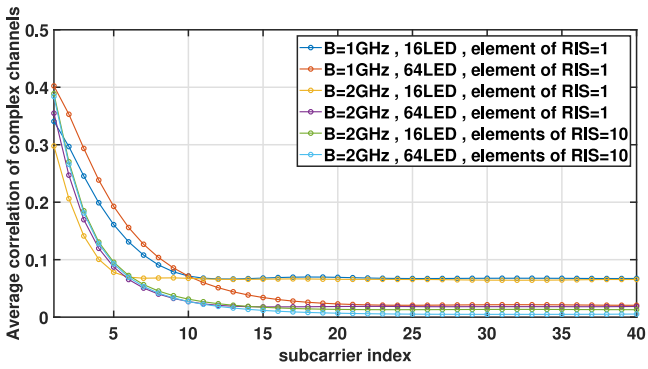

Fig. 5. Average correlation of complex channels.

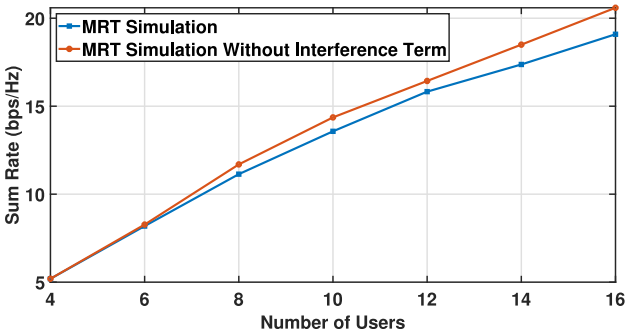

Fig. 6. Sum rate in simulation mode and SNR relation.

method, we will leverage a set of simulation parameters outlined in Table 1.

The LEDs on the ceiling are arranged in a uniform grid. The spacing between the LEDs adjusts based on the total number of LEDs installed. In other words, more LEDs lead to a denser grid to maintain even coverage across the ceiling. Detailed user locations within the room are specified elsewhere in the document. However, for this analysis, we assume a general user height of 0.6 m.

6.1. Average channel correlation

This section dives into a technical detail related to the average correlation of the complex channels. The average correlation for the kth subcarrier is calculated using $\eta_k = E[\frac{|[H_k A_k]_{p,l}|^2}{|[H_k A_k]_{p,p}|^2}]$ where H_k and A_k represent the total channel responses and precoding matrices for the kth subcarrier, respectively. $|[H_k A_k]_{p,l}|^2$ refers to the interference between users. $|[H_k A_k]_{p,p}|^2$ refers to the desired signal for each user. This formula essentially calculates the average ratio between the power of user interference and the power of each user's desired signal.

Fig. 4 depicts a histogram that visualizes the distribution of channel phases between a single LED and a user for various subcarriers. This data was generated by simulating user location changes 10,000 times. The goal is to understand how the channel phase behaves for different subcarriers under user mobility. The horizontal axis represents the channel phase, ranging from 0 to π. The distribution of channel phases across subcarriers reveals a clear trend: In lower subcarriers, the phases are not uniformly distributed. This indicates that user movement has minimal impact on the phase in these subcarriers. The signal propagation through the channel is less sensitive to slight changes in user location. Conversely, for higher subcarriers, the phase distribution becomes more uniform. This suggests that even minor user movements can cause significant changes in the phase. As a result, higher subcarriers are more susceptible to user mobility, leading to less predictable signal behavior and potentially reduced interference between users due to phase cancellation effects.

To investigate the impact of subcarrier index on channel correlation, Fig. 5 explores how the average correlation between complex channels changes across different subcarriers for a system with 16 users. The X-axis represents the subcarrier index, and the Y-axis represents the correlation value. The average correlation between complex channels generally weakens as the subcarrier index increases, regardless of the specific bandwidth used. This indicates that signals transmitted on higher-numbered subcarriers experience less correlation (interaction) with each other compared to lower-numbered subcarriers. This decrease in correlation becomes more pronounced with several factors: A larger number of LEDs transmitting signals leads to a stronger decorrelation effect across subcarriers. The presence of more RIS elements in the signal path further enhances the decorrelation between channels for different subcarriers. Wider bandwidths introduce larger phase differences between the channels compared to simply increasing the subcarrier index. This results in a more rapid decrease in the average correlation as bandwidth increases.

Fig. 6 explores how the number of users in a room affects the achievable sum rate. Due to the specific system setup, MRT precoding and high bandwidth, we assumed minimal user interference for simplification purposes. Room dimensions is $5 \times 5 \times 3$ m^3. A reflective RIS with 20 elements is on one wall. No direct line of sight is between LEDs and users and all signals are reflected by RIS. There are 64 LEDs, User locations were randomized 100 times by Monte Carlo simulation to account for user mobility, and the sum rate was averaged for each number of users. The sum rate remains high with a small number of users, indicating minimal interference between them. As the number of users increases and they become closer to each other, the sum rate starts to decrease due to growing user interference. This highlights the impact of user density on system performance. In essence, the figure demonstrates that while the initial setup minimizes user interference, introducing a larger number of users in close proximity can lead to performance degradation due to increased interference.

6.2. Sum rate maximization

Fig. 7 illustrates the relationship between the number of LEDs in an AP and the achievable sum rate under various operating modes. Different lines on the graph represent distinct modes, including:

- Optimized: The optimal mode determined through optimization techniques.
- Mode Selection: Various combinations of reflect and transmit modes for the STAR-RIS elements (Mode Selection All Reflect: All STAR-RIS elements are in reflect mode, Mode Selection All Transmit: All STAR-RIS elements are in transmit mode, Mode

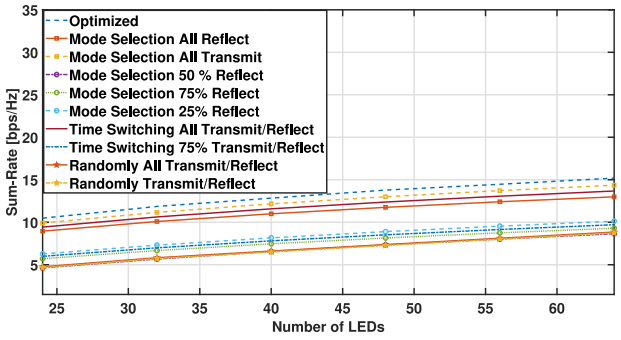

Fig. 7. Sum rate for different number of LEDs.

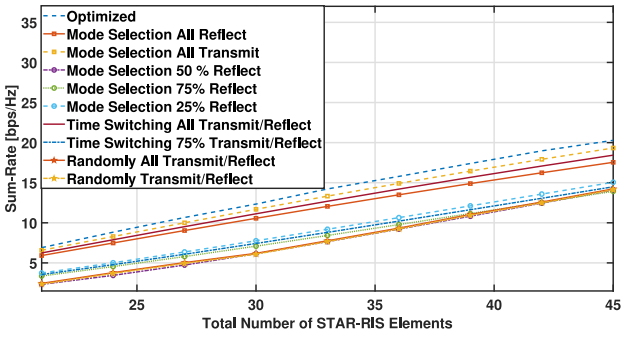

Fig. 8. Sum rate for STAR-RIS with different number of elements.

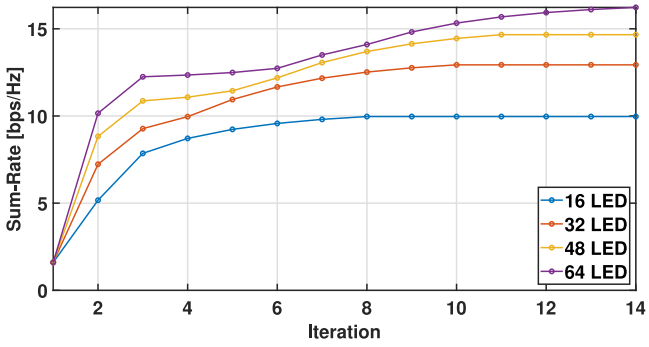

Fig. 9. Number of iterations of the proposed iteration algorithm for different number of LEDs.

Selection 50% Reflect: STAR-RIS elements are in 50% reflect and 50% transmit mode, Mode Selection 75% Reflect: STAR-RIS elements are in 75% reflect and 25% transmit mode, Mode Selection 25% Reflect: STAR-RIS elements are in 25% reflect and 75% transmit mode).

- Time Switching: Periodic switching between transmit and reflect modes (Time Switching All Transmit/Reflect: All STAR-RIS elements switch between transmit and reflect modes over time, Time Switching 75% Transmit/Reflect: STAR-RIS elements switch between 75% transmit/25% reflect and 25% transmit/75% reflect modes over time).
- Random: Random selection of transmit or reflect modes (Randomly All Transmit/Reflect: All STAR-RIS elements randomly transmit and reflect with random percents, Randomly Transmit/Reflect: All STAR-RIS elements randomly transmit or reflect).

The experiment involved a STAR-RIS with 35 elements positioned between two rooms, each with 8 randomly positioned users. To account for user mobility, user positions were randomized 20 times, and the average sum rate was calculated for each LED count. Overall, increasing the number of LEDs generally leads to a higher sum rate as more potential signal paths become available. However, due to the limited total power budget of the AP, this growth eventually saturates. Adding more LEDs beyond this point provides diminishing returns. A key finding is the substantial performance advantage of the optimized configuration compared to other STAR-RIS settings: at least about 1 bps/Hz improvement in sum rate. This demonstrates the importance of tailoring reflection and transmission coefficients for each element to maximize performance. Among the other modes, Mode Selection All Transmit consistently outperforms Mode Selection All Reflect. Time Switching modes generally fall between these two, with Time Switching All Transmit/Reflect performing better than Mode Selection All Reflect. Mode Selection 50% Reflect, Randomly All Transmit/Reflect, and Randomly Transmit/Reflect exhibit similar performance.

Fig. 8 examines how the number of elements in a STAR-RIS system influences the achievable sum rate. With a fixed number of users (16, 8 in each room), the number of LEDs in the first room was set to 64, and user positions were randomized. Similar to Fig. 7, the optimized configuration consistently outperforms other defined STAR-RIS settings, demonstrating the benefits of tailored element coefficients: at least 1 bps/Hz improvement in sum rate. The sum rate generally increases with a larger number of STAR-RIS elements due to the additional signal paths provided. However, this increase comes at the cost of increased computational complexity. As more elements are added, the number of channels and precoding operations grows, making optimization more challenging. The figure highlights the trade-off between higher sum rates and computational complexity. Mode Selection All Transmit consistently achieves the highest performance, while Time Switching All Transmit/Reflect falls between Mode Selection All Transmit and Mode Selection All Reflect. Time Switching 75% Transmit/Reflect performs between Mode Selection 25% Reflect and Mode Selection 75% Reflect. Mode Selection 50% Reflect, Randomly All Transmit/Reflect, and Randomly Transmit/Reflect exhibit similar performance.

Fig. 9 investigates how the number of LEDs in the AP affects the speed at which the optimization algorithm converges. Convergence refers to the algorithm's ability to find the optimal solution. A faster convergence time indicates the algorithm reaches the optimal point quicker. The number of LEDs has a direct impact on the convergence speed of the algorithm. As the number of LEDs increases, the calculations involved become more complex. This complexity translates to a longer time for the algorithm to reach the optimal solution. For example, the figure might show that with a smaller number of LEDs, e.g., 16, the algorithm converges in fewer iterations, e.g., 8, compared to a larger number of LEDs, e.g., 64 which might require more iterations, e.g., 14, to converge. In essence, this figure highlights the trade-off between using a larger number of LEDs for potentially better performance and the increased computational complexity and convergence time associated with it.

7. Conclusion

This paper explored a novel approach for VLC systems that incorporates multiple users, massive MIMO structure, and STAR-RIS. We established a model for this system, including the channel characteristics between light sources, reflectors, and users. To minimize user signal interference, a specific precoding technique called MRT was employed. The core challenge addressed was maximizing the overall data rate for all users. We formulated an optimization problem that involves adjusting the reflection and transmission coefficients of the STAR-RIS elements. Initially, the optimization problem was not solvable using standard techniques. We addressed this by transforming the problem into a convex form using first-order Taylor expansion. This

allowed us to solve the problem effectively using an iterative algorithm. We investigated how the correlation between different user channels behaves under various conditions. We compared the achievable sum rate under different scenarios: Optimal configuration obtained by solving the optimization problem, and non-optimal configurations with fixed or random STAR-RIS coefficients. The results demonstrate that the optimized configuration significantly outperforms the non-optimal approaches and obtains at least around 1 bps/Hz improvement in sum rate. The computational time required for the optimization algorithm increases with a larger number of LEDs. Finally, we explored how the number of users in the system affects the overall data rate. As the user density increases, user interference becomes a more significant factor, and the sum rate decreases. In conclusion, this paper proposes and analyzes a promising approach for VLC systems that leverages STAR-RIS technology to optimize data rate and user experience.

CRediT authorship contribution statement

M.A. Amirabadi: Writing – review & editing, Writing – original draft, Validation, Investigation, Formal analysis, Data curation, Conceptualization. **S.A. Nezamalhosseini:** Writing – review & editing, Validation, Supervision, Conceptualization.

Declaration of competing interest

All authors have participated in (a) conception and design, or analysis and interpretation of the data; (b) drafting the article or revising it critically for important intellectual content; and (c) approval of the final version.

This manuscript has not been submitted to, nor is under review at, another journal or other publishing venue.

The authors have no affiliation with any organization with a direct or indirect financial interest in the subject matter discussed in the manuscript.

Data availability

No data was used for the research described in the article.

References

[1] L.E.M. Matheus, A.B. Vieira, L.F. Vieira, M.A. Vieira, O. Gnawali, Visible light communication: concepts, applications and challenges, IEEE Commun. Surv. Tutor. 21 (4) (2019) 3204–3237.

[2] M. Obeed, A.M. Salhab, M.S. Alouini, S.A. Zummo, On optimizing VLC networks for downlink multi-user transmission: A survey, IEEE Commun. Surv. Tutor. 21 (3) (2019) 2947–2976.

[3] S.H. Younus, A.A. Al-Hameed, M. Alhartomi, A.T. Hussein, Massive MIMO for indoor VLC systems, in: 2020 22nd International Conference on Transparent Optical Networks, ICTON, IEEE, 2020, pp. 1–6.

[4] S.D. Dissanayake, J. Armstrong, Comparison of aco-ofdm, dco-ofdm and ado-ofdm in im/dd systems, J. Lightwave Technol. 31 (7) (2013) 1063–1072.

[5] H. Abumarshoud, L. Mohjazi, O.A. Dobre, M. Di Renzo, M.A. Imran, H. Haas, Lifi through reconfigurable intelligent surfaces: A new frontier for 6G? IEEE Veh. Technol. Mag. 17 (1) (2021) 37–46.

[6] S. Aboagye, A.R. Ndjiongue, T.M. Ngatched, O.A. Dobre, H.V. Poor, RIS-assisted visible light communication systems: A tutorial, IEEE Commun. Surv. Tutor. 25 (1) (2022) 251–288.

[7] A.R. Ndjiongue, T.M. Ngatched, O.A. Dobre, H. Haas, Re-configurable intelligent surface-based VLC receivers using tunable liquid-crystals: The concept, J. Lightwave Technol. 39 (10) (2021) 3193–3200.

[8] A.M. Abdelhady, A.K.S. Salem, O. Amin, B. Shihada, M.S. Alouini, Visible light communications via intelligent reflecting surfaces: Meta-surfaces vs mirror arrays, IEEE Open J. Commun. Soc. 2 (2020) 1–20.

[9] A.M. Abdelhady, O. Amin, A.K.S. Salem, M.S. Alouini, B. Shihada, Channel characterization of IRS-based visible light communication systems, IEEE Trans. Commun. 70 (3) (2022) 1913–1926.

[10] A.R. Ndjiongue, T.M. Ngatched, O.A. Dobre, On the capacity of RIS-assisted intensity-modulation optical channels, IEEE Commun. Lett. 26 (2) (2021) 389–393.

[11] P.P. Játiva, F. Seguel, P. Adasme, Evaluation of intelligent reflecting surfaces for diffuse visible light communications link, in: 2020 IEEE Latin-American Conference on Communications, LATINCOM, IEEE, 2020, pp. 1–5.

[12] S. Aboagye, T.M. Ngatched, O.A. Dobre, A.R. Ndjiongue, Intelligent reflecting surface-aided indoor visible light communication systems, IEEE Commun. Lett. 25 (12) (2021) 3913–3917.

[13] S. Sun, F. Yang, J. Song, R. Zhang, Intelligent reflecting surface for MIMO VLC: Joint design of surface configuration and transceiver signal processing, IEEE Trans. Wireless Commun. 22 (9) (2023) 5785–5799.

[14] S. Sun, F. Yang, J. Song, Sum rate maximization for intelligent reflecting surface-aided visible light communications, IEEE Commun. Lett. 25 (11) (2021) 3619–3623.

[15] B. Cao, M. Chen, Z. Yang, M. Zhang, J. Zhao, M. Chen, Reflecting the light: Energy efficient visible light communication with reconfigurable intelligent surface, in: 2020 IEEE 92nd Vehicular Technology Conference, VTC2020-Fall, IEEE, 2020, pp. 1–5.

[16] L. Qian, X. Chi, L. Zhao, A. Chaaban, Secure visible light communications via intelligent reflecting surfaces, in: ICC 2021-IEEE International Conference on Communications, IEEE, 2021, pp. 1–6.

[17] H. Abumarshoud, B. Selim, M. Tatipamula, H. Haas, Intelligent reflecting surfaces for enhanced NOMA-based visible light communications, in: ICC 2022-IEEE International Conference on Communications, IEEE, 2022, pp. 571–576.

[18] A. Rabiepoor, S.A. Nezamalhosseini, L.R. Chen, IRS-assisted vehicular visible light communications systems: channel modeling and performance analysis, Appl. Opt. 63 (1) (2023) 167–178.

[19] J. Xu, Y. Liu, X. Mu, O.A. Dobre, STAR-RISs: Simultaneous transmitting and reflecting reconfigurable intelligent surfaces, IEEE Commun. Lett. 25 (9) (2021) 3134–3138.

[20] Y. Liu, X. Mu, J. Xu, R. Schober, Y. Hao, H.V. Poor, L. Hanzo, STAR: Simultaneous transmission and reflection for omnidirectional coverage by intelligent surfaces, IEEE Wirel. Commun. 28 (6) (2021) 102–109.

[21] Y. Wang, P. Guan, H. Yu, Y. Zhao, Transmit power optimization of simultaneous transmission and reflection RIS assisted full-duplex communications, IEEE Access 10 (2022) 61192–61200.

[22] M. Ahmed, A. Wahid, S.S. Laique, W.U. Khan, A. Ihsan, F. Xu, Z. Han, A survey on STAR-RIS: Use cases, recent advances, and future research challenges, IEEE Internet Things J. 10 (16) (2023) 14689–14711.

[23] X. Mu, Y. Liu, L. Guo, J. Lin, R. Schober, Simultaneously transmitting and reflecting (STAR) RIS aided wireless communications, IEEE Trans. Wireless Commun. 21 (5) (2021) 3083–3098.

[24] T. Zhou, K. Xu, G. Hu, X. Xia, W. Xie, C. Li, Robust beamforming design for STAR-RIS-assisted anti-jamming and secure transmission, IEEE Trans. Green Commun. Netw. (2023).

[25] Z. Zhu, J. Li, J. Yang, B. Ai, Robust beamforming design for STAR-RIS-aided secure SWIPT system with bounded CSI error, IEEE Trans. Green Commun. Netw. (2024).

[26] Z. Zhu, Z. Li, Z. Chu, Y. Guan, Q. Wu, P. Xiao, et al., Intelligent reflecting surface assisted mm-wave integrated sensing and communication systems, IEEE Internet Things J. (2024).

[27] X. Lv, S. Rani, S. Manimurugan, A. Slowik, Y. Feng, Quantum-inspired sensitive data measurement and secure transmission in 5G-enabled healthcare systems, Tsinghua Sci. Technol. (2024).

[28] Z. Zhu, Z. Li, Z. Chu, Q. Wu, J. Liang, Y. Xiao, et al., Intelligent reflecting surface-assisted wireless powered heterogeneous networks, IEEE Trans. Wireless Commun. 22 (12) (2023) 9881–9892.

[29] Z. Zhu, Z. Li, Z. Chu, G. Sun, W. Hao, P. Liu, I. Lee, Resource allocation for intelligent reflecting surface assisted wireless powered IoT systems with power splitting, IEEE Trans. Wireless Commun. 21 (5) (2021) 2987–2998.

[30] A.R. Ndjiongue, T.M. Ngatched, O.A. Dobre, H. Haas, H. Shin, Double-sided beamforming in VLC systems using omni-digital reconfigurable intelligent surfaces, IEEE Commun. Mag. 62 (2) (2023) 150–155.

[31] A. Salehiyan, M.J. Emadi, Performance analysis of uplink optical wireless communications in the presence of a simultaneously transmitting and reflecting reconfigurable intelligent surface, IET Optoelectron. 17 (4) (2023) 129–138.

[32] M.J. Zakavi, S.A. Nezamalhosseini, L.R. Chen, Multiuser massive MIMO-OFDM for visible light communication systems, IEEE Access 11 (2023) 2259–2273.

[33] S. Sun, F. Yang, J. Song, R. Zhang, Intelligent reflecting surface for MIMO VLC: Joint design of surface configuration and transceiver signal processing, IEEE Trans. Wireless Commun. 22 (9) (2023) 5785–5799.

[34] C. Chen, S. Huang, H. Abumarshoud, I. Tavakkolnia, M. Safari, H. Haas, Frequency-domain channel characteristics of intelligent reflecting surface assisted visible light communication, J. Lightwave Technol. (2023).

[35] H. Shen, Y. Deng, W. Xu, C. Zhao, Rate maximization for downlink multiuser visible light communications, IEEE Access 4 (2016) 6567–6573.

[36] M.G. Kibria, H. Murata, S. Yoshida, An efficient algorithm for weighted sum-rate maximization in multicell OFDMA downlink, IEICE Trans. Fundam. Electron. Commun. Comput. Sci. 97 (1) (2014) 69–77.

[37] L.N. Tran, M.F. Hanif, A. Tolli, M. Juntti, Fast converging algorithm for weighted sum rate maximization in multicell MISO downlink, IEEE Signal Process. Lett. 19 (12) (2012) 872–875.

[38] S. Dhok, P.K. Sharma, Rate-splitting multiple access with STAR RIS over spatially-correlated channels, IEEE Trans. Commun. 70 (10) (2022) 6410–6424.
[39] X. Mu, Y. Liu, L. Guo, J. Lin, R. Schober, Simultaneously transmitting and reflecting (STAR) RIS aided wireless communications, IEEE Trans. Wireless Commun. 21 (5) (2021) 3083–3098.
[40] M. Katwe, K. Singh, B. Clerckx, C.P. Li, Improved spectral efficiency in STAR-RIS aided uplink communication using rate splitting multiple access, IEEE Trans. Wireless Commun. 22 (8) (2023) 5365–5382.
[41] F. Kaltenberger, D. Gesbert, R. Knopp, M. Kountouris, Correlation and capacity of measured multi-user MIMO channels, in: 2008 IEEE 19th International Symposium on Personal, Indoor and Mobile Radio Communications, IEEE, 2008, pp. 1–5.
[42] H. Shen, Y. Deng, W. Xu, C. Zhao, Rate-maximized zero-forcing beamforming for VLC multiuser MISO downlinks, IEEE Photonics J. 8 (1) (2016) 1–13.
[43] M. Yang, Y. Chen, L. Du, J. Wang, X. Zhang, Secrecy energy efficiency optimization for multiuser massive MIMO wiretap systems with transmit antenna selection, Phys. Commun. 59 (2023) 102101.
[44] Z. Wei, C. Masouros, Device-centric distributed antenna transmission: Secure precoding and antenna selection with interference exploitation, IEEE Internet Things J. 7 (3) (2019) 2293–2308.
[45] S. Boyd, L. Vandenberghe, Convex Optimization, Cambridge University Press, 2004.

Mohammad Ali Amirabadi was born in Zahedan, Iran, in 1993. He received the B.Sc. degree in Optics & Laser Engineering from Malek-e-Ashtar University of Technology, Isfahan, Iran, in 2015, and the M.Sc.,Ph.D. and Postdoc degrees in Communication Engineering from Iran University of Science and Technology, Tehran, Iran in 2017, 2022, and 2023, respectively. Now he is an Assistant Professor in Communication Engineering group at Ferdowsi university of Mashhad, Mashhad, Iran. His research interests include Optical Communications.

S. Alireza Nezamalhosseini received the B.Sc. degree in electrical engineering from Amirkabir University of Technology, Tehran, Iran, in 2006, and the M.Sc. and Ph.D. degrees in electrical engineering from Sharif University of Technology (SUT), Tehran, Iran, in 2008 and 2013, respectively. He is currently an assistant professor at Iran University of Science and Technology (IUST), Tehran. His research interests include underwater wireless optical communications, mode-division multiplexing in optical fibers, and visible light communications.